XL CILAMCE
IBERO-LATIN AMERICAN CONGRESS ON COMPUTATIONAL METHODS IN ENGINEERING
NOVEMBER 11-14, 2019
Praiamar Natal Hotel & Convention
Natal, RN-BRAZIL

NUMERICAL EVALUATION OF MICROPOLAR ELASTIC PARAMETERS FOR A HETEROGENEOUS MICROSTRUCTURE

Raphael A. R. Medeiros
Roque L. S. Pitangueira
Lapo Gori
raphaelrochamedeiros@ufmg.br
roque@dees.ufmg.br
lapo@dees.ufmg.br
Department of Structural Engineering, Federal University of Minas Gerais
Av. Antônio Carlos, 6627, Pampulha, 31270-901, Belo Horizonte, MG, Brasil

Abstract. Materials that, like concrete, possess a heterogeneous microstructure, are characterized by behaviours at the macroscale that are difficult to be represented with standard continuum descriptions. Generalized continua models, due to their enriched kinematical description, are well-suited for the representation of microstructural effects. The main limitation to the use of generalized models is the presence of additional material parameters, difficult to be obtained through experiments. The present work deals with the definition of the two additional parameters of the micropolar continuum theory, using a numerical homogenization strategy. The main aim is, then, to obtain an equivalent micropolar macromedium starting from a random heterogeneous microstructure. This paper focuses on a homogenization strategy originally conceived for periodic microstructures, and presents a preliminary investigation on its extension to randon heterogeneous microstructures. The theoretical aspects are discussed, and some initial numerical results are presented.

Keywords: Heterogeneous media; Homogenization; Micropolar media

1 Introduction

Continuum mechanics is based on the premise that constitutive laws allow the description of a material's response when its strain or stress history is known. Said response depends on constitutive parameters that may vary along the body and, if this variation occurs in small scales, it can be of difficult mathematical treatment and experimental observation. According to Fuina [1], it's possible to determine the aforementioned parameters by analysing stresses and strains in a Representative Volume Element (RVE), which must be larger than the material's non-homogeneities.

In the analysis of heterogeneous media, given the importance of the kinematic hypotheses and of those associated with the material's constitutive response, it is important that there are theories conceived considering relevant aspects of the material's microstructure. This is not the case of the classical continuum theory (Cauchy's continuum), not appropriate to the analysis of materials with complex microstructures.

Several theories were developed in order to analyse materials with complex microstructures and, in their formulation, the behaviour of the material at the microscale is taken into account. Such theories are known as *generalized continua* or *higher-order* continua theories and, dividing them into two large groups, there are those that consider higher-order displacement gradients while the others endow the material particles with additional kinematic degrees of freedom.

According to Eringen [2], generalized continua theories treat a material body as continuous collection of material point particles, the so-called microcontinua. The higher-order displacement gradients or the additional degrees of freedom aim to represent the deformability of the material particles.

In the micromorphic continuum theory, for example, the material particles have nine additional degrees of freedom, allowing the analysis of materials whose microstructure can deform arbitrarily, like polymers with flexible molecules, animal blood with deformable cells, turbulent fluids with flexible vortices, etc. There are particular cases of micromorphic continua that, with simpler formulations, are well-suited to analysis of media whose deformations have some kind of restriction. The classical continuum itself may be understood as a very particular case of micromorphic continuum, with particles having only three translations as kinematic degrees of freedom.

Another particular case of micromorphic continuum is the micropolar continuum, also known as Cosserat continuum, appropriate to the analysis of materials with rigid microstructures, as in this theory the material particles cannot undergo any change in shape or volume, being subjected to only three additional degrees of freedom, which are rigid body rotations, referred to as microrotations.

However, while it is known that a micropolar medium model is superior to a classical model for the analysis of several materials, determining the size of the representative volume element for a heterogeneous micropolar media has been an obstacle so far, specially when the materials have random microstructures, as Trovalusci et al. [3] point out.

Another point that stands out and hinders the practical use of generalized continua is that, while for the classical continuum the constitutive parameters of the materials are already well established and have a physical meaning easily observable, the additional parameters that arise when using higher-order continua theories do not always have clear physical meaning or can be obtained through experiments.

Thus, this work presents a numerical strategy for obtaining a homogeneous micropolar continuum from a medium described as a classical continuum with a heterogeneous microstructure, not necessarily periodical. All components of the constitutive tensors of the material, treated as micropolar in the macroscale, are obtained from the parameters of a Cauchy continuum.

2 Theoretical foundation

According to Monteiro et al. [4], all materials are heterogeneous in some sufficiently small length scale and in the case of quasi-brittle media, such as mortar and concrete, the non-homogeneous nature of the continuum is responsible for many of the phenomena captured in structural level, especially the non-linear mechanical behaviour. Lemaitre and Desmorat [5] define brittle materials as those that break

without any irreversible strains and without any dissipation prior to cracking (e.g., glass and some ceramics). A material is considered quasi-brittle when a dissipation prior to cracking exists with no or negligible permanent strains. To analyse such materials and others with different organizations in microstructural level, there are several theories that can be used to obtain satisfactory results.

Although since the late nineteenth century there have been records of the first studies aimed at introducing the effects of the materials microstructure on elasticity, it was mainly from the 1960s that much was published about generalized continua.

One of the generalized continua theories is the micropolar continuum theory, or Cosserat continuum theory, whose kinematics and strain measures are briefly discussed in this section.

2.1 Micropolar continuum kinematics

In classical continuum mechanics, it is understood that the points of a body are undeformable and subjected only to translational movements. Figure 1 shows this movement for a generic point, P, of a body.

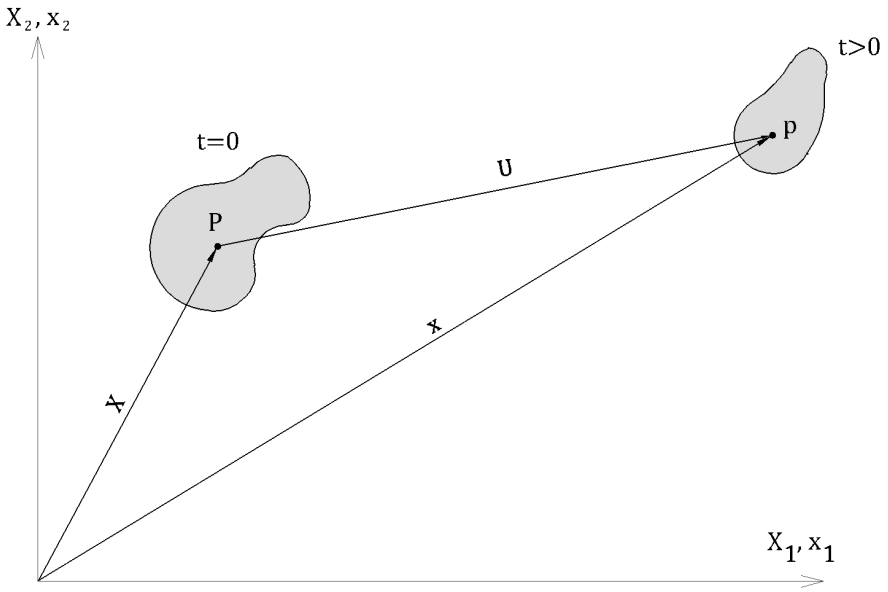

Figure 1. Classical continuum kinematics.

The point P, initially in a position $\mathbf{X}$ in the body's undeformed configuration (instant $t = 0$), occupies a position $\mathbf{x}$ in its deformed, or spatial configuration ($t > 0$). The translation, the rigid body rotation and the shape change undergone by the body are described based on the relation between $\mathbf{X}$ and $\mathbf{x}$. Note that no consideration whatsoever is made about the material's microstructure.

For a micropolar continuum, although, the points of a body are treated as material particles and are no longer subject only to translational movements. As figure 2 illustrates, there is a small region around the point P , which can be treated as a continuum medium. The region is called a microcontinuum and can undergo a translational motion (represented by $\mathbf{U}$) and a rigid body rotation, $\mathbf{\Phi}$. Said rotation of the material particle is known as microrotation and may differ from the body's macrorotation.

Imposing that the material particle is subjected to rigid body translations and rotations that do not alter its shape or volume is a particularity of the micropolar continuum. Different theories attribute other degrees of freedom to the particles, e.g., shear deformations, expansion and contraction.

Figure 3, illustrates the kinematics of the micropolar particles in detail and then its formulation is

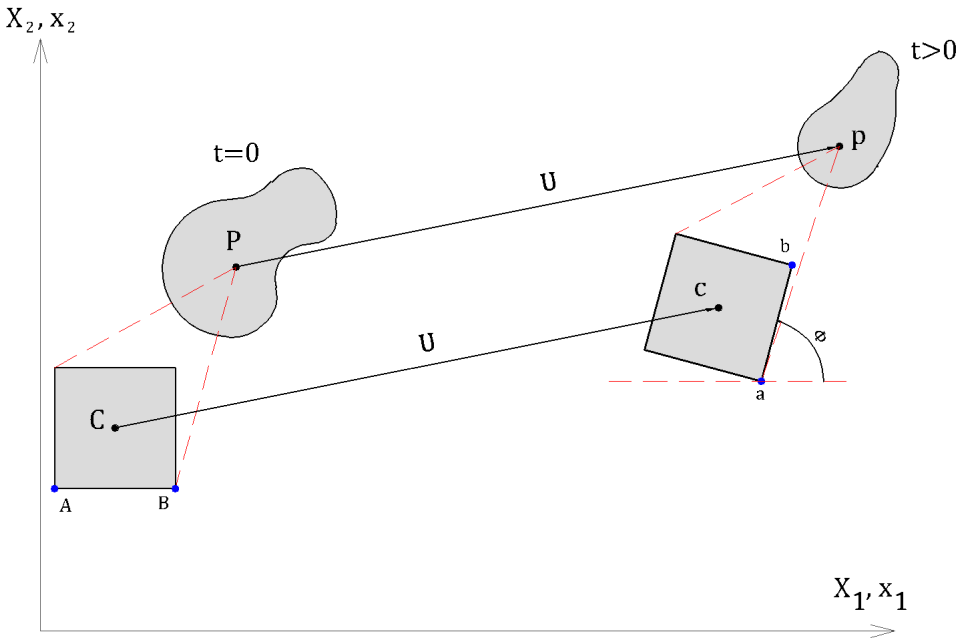

Figure 2. Micropolar continuum kinematics.

discussed.

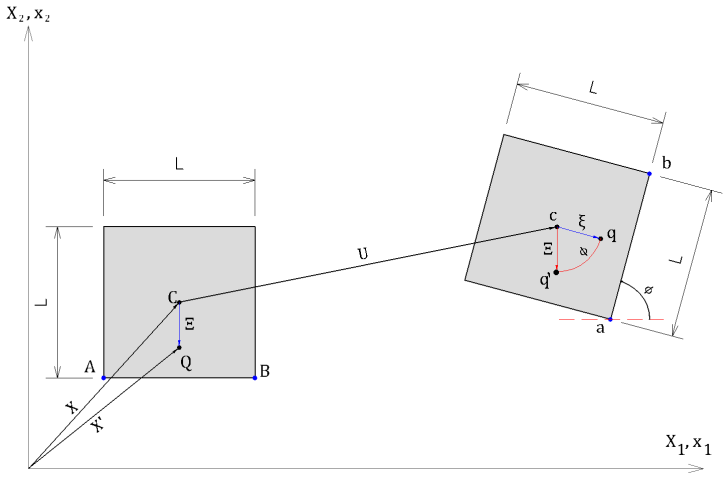

Figure 3. Micro Rotation undergone by a micropolar particle shown in detail.

Consider that a vector, $\boldsymbol{\Xi}$, is attached to the particle's centroid, C, connecting it to another point, Q. When the body deforms, the vector $\boldsymbol{\Xi}$ becomes the vector $\boldsymbol{\xi}$, which connects the points c and q of the microcontinuum in its spatial configuration. This transformation is described by equation 1, as follows:

$$\boldsymbol{\xi} = \boldsymbol{\chi}\boldsymbol{\Xi}, \tag{1}$$

where $\boldsymbol{\chi}$ is known as microdeformation tensor and, for the micropolar continuum, consists of a rotation

tensor responsible for changing the direction of $\boldsymbol{\Xi}$, but not its norm.

For small microrotations, equation (1) may be rewritten as below:

$$\boldsymbol{\xi} = \boldsymbol{\Xi} + \boldsymbol{\Phi} \times \boldsymbol{\Xi}, \tag{2}$$

the cross product $\boldsymbol{\Phi} \times \boldsymbol{\Xi}$ approximating the vector that connects the points q' and q in figure 3.

2.2 Strain measures

For centro-symmetric, elastic, linear micropolar media, the deformation tensors have the following components:

$$\gamma_{ij} = U_{j,i} - \epsilon_{ijk}\Phi_k; \tag{3}$$

$$\kappa_{ij} = \Phi_{j,i}. \tag{4}$$

In equations (3) and (4), γ_{ij} are the components of the *strain tensor*, κ_{ij} are the components of the *microcurvature tensor* and the symbol ϵ_{ijk} indicates the components of the standard Levi-Civita operator with three indexes. Tensor $\boldsymbol{\gamma}$ is related to distortions and variations in dimensions, while $\boldsymbol{\kappa}$ is related to curvatures and torsions of the microstructure.

It is interesting to note that $\boldsymbol{\gamma}$ can be decomposed into a symmetric part, $\gamma_{(ij)}$ and a skew-symmetric part, $\gamma_{\langle ij \rangle}$:

$$\gamma_{(ij)} = \frac{1}{2}(U_{j,i} + U_{i,j}); \tag{5}$$

$$\gamma_{\langle ij \rangle} = \frac{1}{2}(U_{j,i} - U_{i,j}) - \epsilon_{ijk}\Phi_k; \tag{6}$$

The symmetric part of the strain tensor $\boldsymbol{\gamma}$ coincides with the classic strain tensor, $\boldsymbol{\varepsilon}$, while the skew-symmetric part equals to the difference between the macrorotation tensor, $\boldsymbol{\omega}$, and the microrotation tensor, $\boldsymbol{\Phi}$.

2.3 Stress tensor and couple stress tensor

To the strain and microcurvature tensors correspond, respectively, the stress tensor $\boldsymbol{\sigma}$ and the couple-stress tensor $\boldsymbol{\mu}$.

Just like the strain tensor, the stress tensor can be decomposed into a symmetrical part and a skew-symmetric part. The symmetric part of $\boldsymbol{\sigma}$ coincides with the classic Cauchy stress tensor.

2.4 Constitutive relations for the micropolar continuum

For the micropolar continuum, the constitutive relations, which associate stresses to deformations and couple stresses to microcurvatures, are as follows:

$$\sigma_{ij} = D_{ijkl}\gamma_{kl} \tag{7}$$

$$\mu_{ij} = L_{ijkl}\kappa_{kl} \tag{8}$$

The components of the constitutive tensors, D_{ijkl} and L_{ijkl}, depend on the additional parameters of the micropolar continuum and the difficulty of obtaining those parameters is one of the main drawbacks when dealing with the micropolar continuum theory.

3 Strategy for building a micropolar continuum from a classic continuum

A key to the success of many modern structural components is, according to Zohdi and Wriggers [6], the planned behaviour of the material. A relatively inexpensive way to obtain macroscopically desired responses is to enhance a base matrix properties by the addition of microscopic matter, i.e. to manipulate the microstructure. Accordingly, in many modern engineering designs, materials with highly complex microstructures are now in use and the macroscopic characteristics of modified base materials are the aggregate response of an assemblage of different components.

In an attempt to perform a direct numerical simulation, for example, of the mechanical response of a macroscopic structure composed of a material heterogeneous at the microscale, incorporating all of the details of this scale, an extremely mesh would be needed to capture the effects of the microscale heterogeneities.

The resulting system of equations would contain a great number of numerical unknowns and the solution of such a problem could be beyond the capacity of the available computing machines. Thus, the use of *homogenized* materials is common and the usual approach is to determine a constitutive relation between averages, relating volume averaged field variables such as strains and stresses.

The volume averaging takes place over a statistically representative sample of the material, referred to as representative volume element. Hill [7] defines the RVE as a sample of the material that is structurally typical of the the whole mixture on average and contains a sufficient number of inclusions for the apparent material properties to be independent of the surface values of traction and displacement, so long as these values are macroscopically uniform.

The average values of the variables of interest are computed by solving a series of boundary value problems with test loadings. Such regularization processes are referred to as *homogenization* and in this section a numerical strategy is presented so that, from a classical medium with heterogeneous microstructure, an equivalent homogeneous micropolar medium is obtained.

3.1 Boundary conditions

Within the framework of classical homogenization theory, according to Chen et al. [8], the linear boundary condition in the RVE is assumed as $u_i = E_{ij}x_j$ or $\sigma_{ij}n_j = \Sigma_{ij}n_j$, where u_i and σ_{ij} are, respectively, the local displacement field and the stress components inside the RVE while E_{ij} and Σ_{ij} are, respectively, the macroscopic strains and stresses applied on the boundary of the RVE.

The aim of the classical homogenization is to replace a heterogeneous material by a classic homogeneous medium using the Hill-Mandel condition:

$$\langle \sigma_{ij}\varepsilon_{ij} \rangle = \Sigma_{ij}E_{ij}, \tag{9}$$

where the operator $\langle * \rangle$, applied to a quantity $*$, means the volume average of $*$ over the RVE.

In order to obtain a homogeneous micropolar continuum from a heterogeneous classical continuum, the approach described by Forest and Sab [9] is adopted, which is based on the systematic construction of relationships between macroscopic higher-order kinematic quantities and local displacements.

The first step of the strategy is to establish a relation between the local displacement field, $\mathbf{u}$, and the macroscopic displacements and microrotations ($\mathbf{U}$ and $\mathbf{\Phi}$). Said relation is constructed using the least square approximation.

The displacement field of an homogenized micropolar element is

$$\mathbf{u}^* = \mathbf{U} + \mathbf{\Phi} \times (\mathbf{X}' - \mathbf{X}). \tag{10}$$

Figure 3 shows the vectors $\mathbf{X}'$ and $\mathbf{X}$, related as follows:

$$\mathbf{\Xi} = \mathbf{X}' - \mathbf{X}. \tag{11}$$

The best fit of $\mathbf{u}^*$ to the RVE's real displacement field is then sought, minimizing the error over the volume of:

$$\Delta = \int_V |\mathbf{u} - \mathbf{u}^*|^2 \, dV. \tag{12}$$

The minimization of Δ considering a cubic RVE with sides of length L leads to:

$$U_i = \langle u_i \rangle; \tag{13}$$

$$\Phi_i = \frac{6}{L^2} \langle \epsilon_{ijk}(x_j - X_j)u_k \rangle. \tag{14}$$

With equations (13), (14) and using equations (4), (5) and (6), it is possible to determine the macroscopic strain components (symmetric and skew-symmetric parts) and the microcurvature components as functions of the local displacement field inside the RVE.

Assuming that the the local displacement field is polynomial, it can be expressed as follows:

$$u_i = A_i + B_{i1}x_1 + B_{i2}x_2 + B_{i3}x_3 + C_{i1}x_1^2 + C_{i2}x_2^2 + +C_{i3}x_3^2 + ... \tag{15}$$

Once the order of the polynomial is defined, its coefficients can be determined using the equations (4), (5), (6), (13) and (14) and providing scale invariance condition: $E_{ij}(X_k) = \varepsilon_{ij}(X_k)$.

If the displacement on the boundary of the RVE is linear, this corresponds to classical homogeneous boundary condition:

$$u_1 = \gamma_{(11)}x_1 + \gamma_{(12)}x_2 + \gamma_{(13)}x_3; \tag{16a}$$

$$u_2 = \gamma_{(21)}x_1 + \gamma_{(22)}x_2 + \gamma_{(23)}x_3; \tag{16b}$$

$$u_3 = \gamma_{(31)}x_1 + \gamma_{(32)}x_2 + \gamma_{(33)}x_3. \tag{16c}$$

Assuming that the displacement is a second-order polynomial leads to:

$$u_1 = -\frac{1}{2}\kappa_{23}x_2^2 + \frac{1}{2}\kappa_{32}x_3^2 - \kappa_{13}x_1x_2 + \kappa_{12}x_1x_3 + \frac{2}{3}(\kappa_{22} - \kappa_{33})x_2x_3; \tag{17a}$$

$$u_2 = \frac{1}{2}\kappa_{13}x_1^2 - \frac{1}{2}\kappa_{31}x_3^2 + \kappa_{23}x_1x_2 - \kappa_{21}x_1x_3 + \frac{2}{3}(\kappa_{33} - \kappa_{11})x_1x_3; \tag{17b}$$

$$u_3 = -\frac{1}{2}\kappa_{12}x_1^2 + \frac{1}{2}\kappa_{21}x_2^2 + \kappa_{31}x_2x_3 - \kappa_{32}x_1x_3 + \frac{2}{3}(\kappa_{11} - \kappa_{22})x_1x_2. \tag{17c}$$

If the displacement field is a third-order polynomial, it can be expressed as:

$$u_1 = 10\left[\theta_3(x_2^3 - 3x_1^2x_2) + \theta_2(3x_1^2x_3 - x_3^3)\right]; \tag{18a}$$

$$u_2 = 10\left[\theta_3(-x_1^3 + 3x_2^2x_1) + \theta_1(-3x_2^2x_3 + x_3^3)\right]; \tag{18b}$$

$$u_3 = 10\left[\theta_2(x_1^3 - 3x_3^2x_1) + \theta_1(3x_3^2x_2 + x_2^3)\right], \tag{18c}$$

where,

$$\theta_i = \frac{1}{2L^2}\epsilon_{ijk}\gamma_{\langle jk \rangle}$$

About the assumption of a complete cubic field to represent the local displacement inside the RVE, the third order polynomial is the minimum in order to include the skew-symmetric strain components.

At last, the overall homogenized micropolar properties can be determined using an extended form of Hill-Mandell condition:

$$\langle \sigma_{ij}\varepsilon_{ij} \rangle = \frac{1}{V}\int_V \sigma_{ij}u_{j,i}dV = \Sigma_{(ij)}\gamma_{(ij)} + M_{ij}\kappa_{ij} + \Sigma_{\langle ij \rangle}\gamma_{\langle ij \rangle} \tag{19}$$

By submitting the previous three sets of local displacements (equations (16), (17) and (18)) into equation (19), it is possible to obtain the macroscopic stresses and couple stresses in terms of the local stress field.

For a plane problem, the energetically active macroscopic stress and couple stress components described as functions of the stress field within the RVE are as follows:

$$\Sigma_{(11)} = \frac{1}{V}\int_V \sigma_{11}dV = \langle \sigma_{11} \rangle; \tag{20a}$$

$$\Sigma_{(12)} = \frac{1}{V}\int_V \sigma_{12}dV = \langle \sigma_{12} \rangle; \tag{20b}$$

$$\Sigma_{(22)} = \frac{1}{V}\int_V \sigma_{22}dV = \langle \sigma_{22} \rangle; \tag{20c}$$

$$M_{13} = \frac{1}{V}\int_V -\sigma_{11}x_2 dV; \tag{20d}$$

$$M_{23} = \frac{1}{V}\int_V \sigma_{22}x_1 dV; \tag{20e}$$

$$\Sigma_{\langle 12 \rangle} = \frac{30}{L^2}\frac{1}{V}\int_V \left[x_1x_2(\sigma_{22} - \sigma_{11}) + \sigma_{12}(x_2^2 - x_1^2)\right] dV. \tag{20f}$$

The boundary conditions presented can be applied to the RVE to determine its stress field and, with the set of equations (20), the macroscopic stress and couple stress components can be computed. Finally, using equations (7) and (8) it is possible to determine the components of the constitutive tensors of the homogenized micropolar material.

4 Application examples

Two examples of application of the proposed strategy are presented in this section . In both of them, the strategy was applied to plane problems, for which the convenient organization of the macroscopic components of stresses and strains in vectors, leads to:

$$\begin{Bmatrix} \Sigma_{(11)} \\ \Sigma_{(22)} \\ \Sigma_{(12)} \\ M_{13} \\ M_{23} \\ \Sigma_{\langle 12 \rangle} \end{Bmatrix} = \begin{bmatrix} c_{11} & \cdots & c_{16} \\ \vdots & \ddots & \vdots \\ c_{61} & \cdots & c_{66} \end{bmatrix} \begin{Bmatrix} \gamma_{(11)} \\ \gamma_{(22)} \\ \gamma_{(12)} \\ \kappa_{13} \\ \kappa_{23} \\ \gamma_{\langle 12 \rangle} \end{Bmatrix} \tag{21}$$

With the size of the RVE and its materials properties determined, the volume element is subjected to the boundary conditions discussed in the previous section (equations (16), (17) e (18)).

In each example, six simulations were required to analyze all the situations in which only one of the energetically active macroscopic strain components had a nonzero value. All these simulations were performed using the Finite Element Method (FEM) and with the aid of INSANE (INteractive Structural

ANalysis Environment), software developed at the Department of Structural Engineering (DEEs) of the Federal University of Minas Gerais (UFMG).

For each case where a vector component on the right-hand side of equation (21) had a predetermined value and the others were all null, the stress field in the EVR was obtained and the macroscopic stress ($\Sigma_{(ij)}$ and $\Sigma_{\langle ij \rangle}$) and couple stress components (M_{ij}) were determined using the set of equations (20).

Finally, the components, c_{ij}, of the constitutive matrix that relates the macroscopic micropolar quantities were obtained, one column at each simulation.

In all the simulations performed, a mesh with 16 four-node quadrilateral elements was used. This mesh guarantees the continuity of the displacements throughout the entire model. The same can't be said about the strains and stresses, which are evaluated at the integration points of the elements. In both examples presented in this section, the figures showing the distribution of stresses inside the RVE are generated using an INSANE post processor feature that smooths the discontinuities in the strain and stress fields.

4.1 Example 1: homogeneous material

For this first example, a square RVE with the following properties was considered:

- length of the sides: 0.1 m;
- Young's modulus of the material: $E = 2.1 \cdot 10^{10}$ N/m^2;
- Poisson's ratio of the material: $\nu = 0.2$.

In the first test on the RVE, it was assigned unit value to the component $\gamma_{(11)}$. In this case, the body assumed the spatial configuration shown in figure 4.

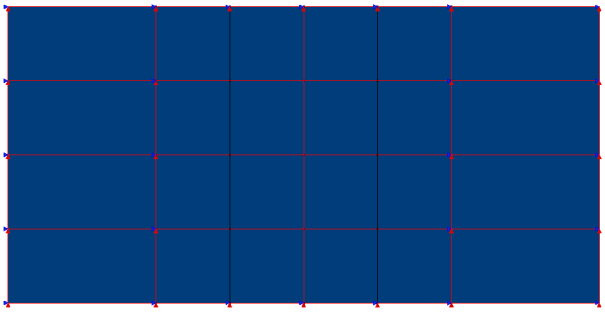

Figure 4. Spatial configuration of the homogeneous RVE for $\gamma_{(11)} = 1$.

In the entire RVE, the stress σ_{12} resulted null and figure 5 shows the distribution of the stresses σ_{11} and σ_{22}, constant and respectively equal to $2.083 \cdot 10^{10}$ N/m^2 and $4.167 \cdot 10^{9}$ N/m^2 throughout the body.

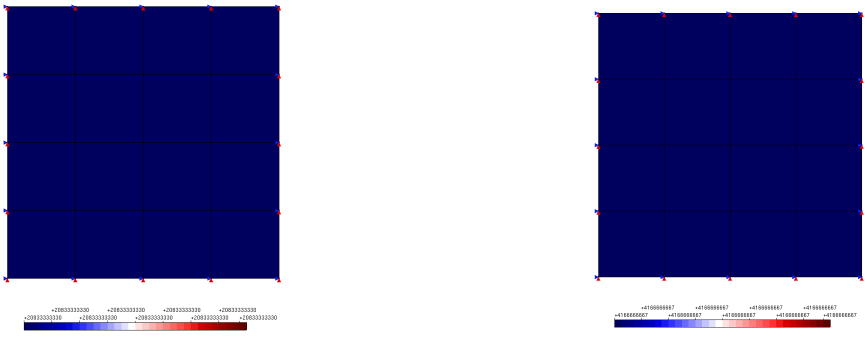

(a) σ_{11} (b) σ_{22}

Figure 5. Stresses σ_{11} and σ_{22} in the homogeneous RVE for $\gamma_{(11)} = 1$.

When $\gamma_{(22)} = 1$ was used, the spatial configuration of the body and the distribution of the stresses σ_{11} and σ_{22} were those presented in figures 6 and 7. Again, σ_{12} resulted null, while σ_{11} and σ_{22} were respectively equal to $4.167 \cdot 10^{9}$ N/m^2 and $2.083 \cdot 10^{10}$ N/m^2 in the whole RVE.

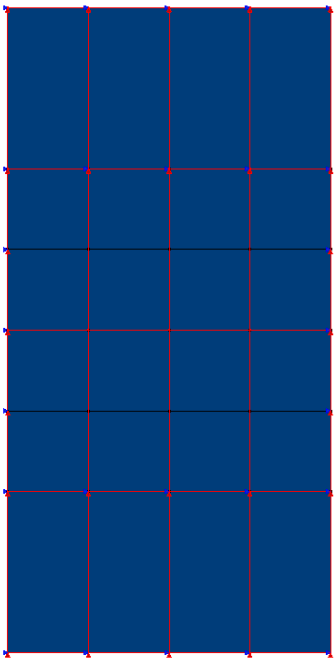

Figure 6. Spatial configuration of the homogeneous RVE for $\gamma_{(22)} = 1$.

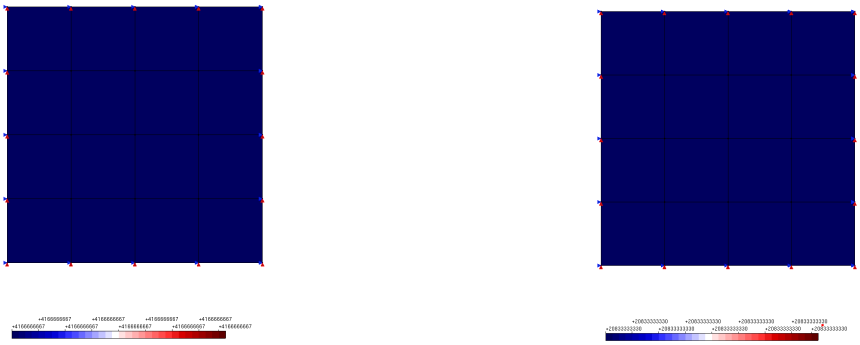

(a) σ_{11} (b) σ_{22}

Figure 7. Stresses σ_{11} and σ_{22} in the homogeneous RVE for $\gamma_{(22)} = 1$.

On the third test, it was determined the value 0.5 for $\gamma_{(12)}$ and the resulting deformed shape of RVE is that of figure 8. In this test, σ_{11} and σ_{22} resulted null, while σ_{12} was constant and equal to $8.333 \cdot 10^9$ N/m^2, as shown in figure 9.

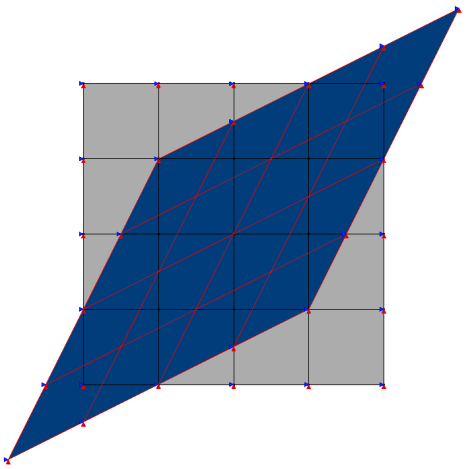

Figure 8. Spatial configuration of the homogeneous RVE for $\gamma_{(12)} = 0.5$.

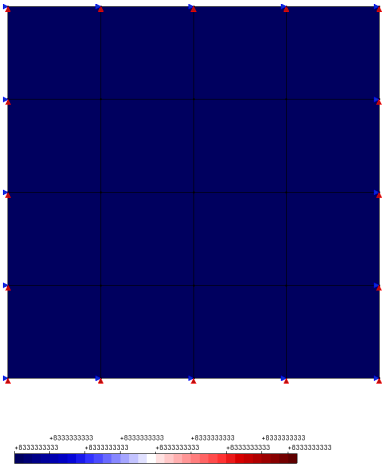

Figure 9. Stress σ_{12} in the homogeneous RVE for $\gamma_{(12)} = 0.5$.

For the fourth test, it was used $\kappa_{13} = 1$. The spatial configuration of the RVE is seen on figure 10. Figure 11 shows the variation of the stresses in the RVE.

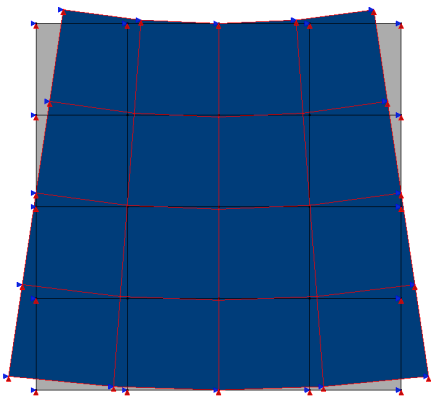

Figure 10. Spatial configuration of the homogeneous RVE for $\kappa_{(13)} = 1$.

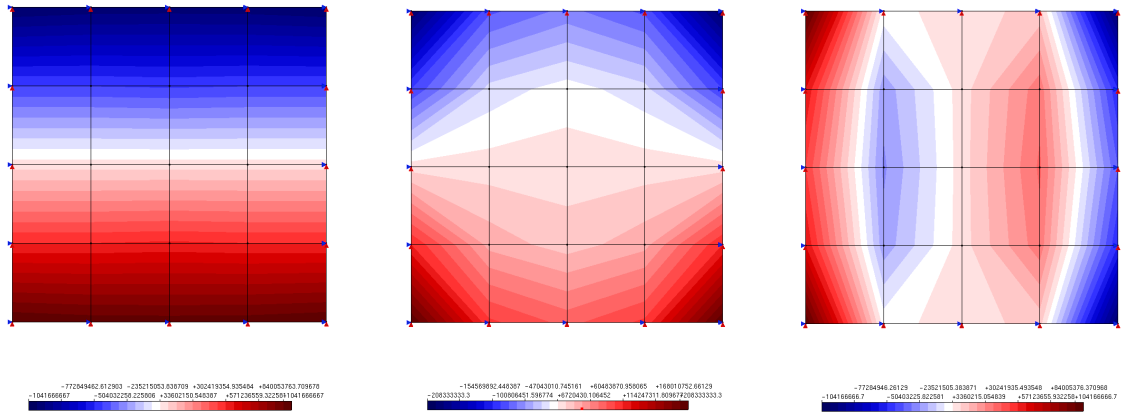

(a) σ_{11} (b) σ_{22} (c) σ_{12}

Figure 11. Stresses σ_{11}, σ_{22} e σ_{12} in the homogeneous RVE for $\kappa_{(13)} = 1$.

For $\kappa_{23} = 1$, the deformed shape of the body and the variation of the stresses in its domain are presented on figures 12 e 13

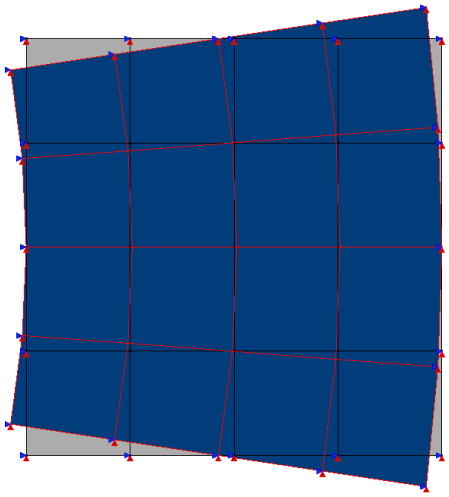

Figure 12. Spatial configuration of the homogeneous RVE for $\kappa_{(23)} = 1$.

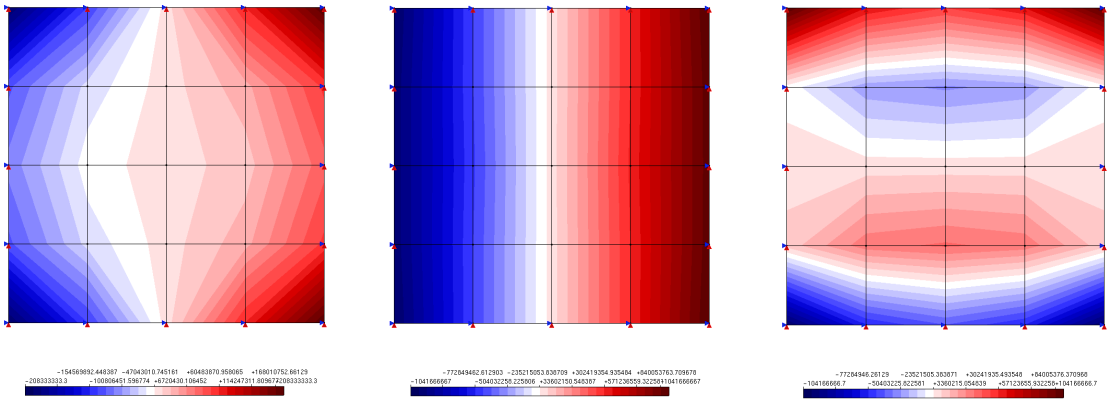

(a) σ_{11} (b) σ_{22} (c) σ_{12}

Figure 13. Stresses σ_{11}, σ_{22} e σ_{12} in the homogeneous RVE for $\kappa_{(23)} = 1$.

On the sixth test, $\gamma_{\langle 12 \rangle} = 0.05$ was adopted, since values close to the unit result in a physically

impossible deformation for the body. Figures 14 and 15 show, respectively, the spatial configuration of the RVE and the variation of the stresses in it.

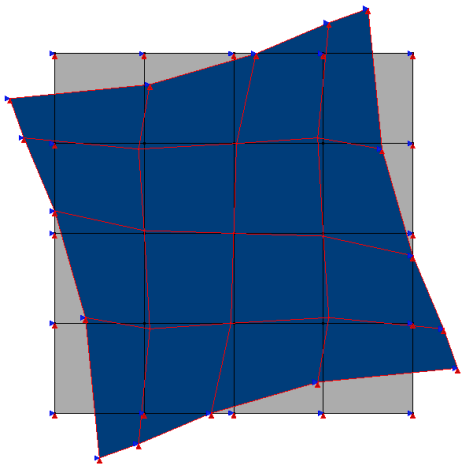

Figure 14. Spatial configuration of the homogeneous RVE for $\gamma_{\langle 12\rangle} = 0.05$.

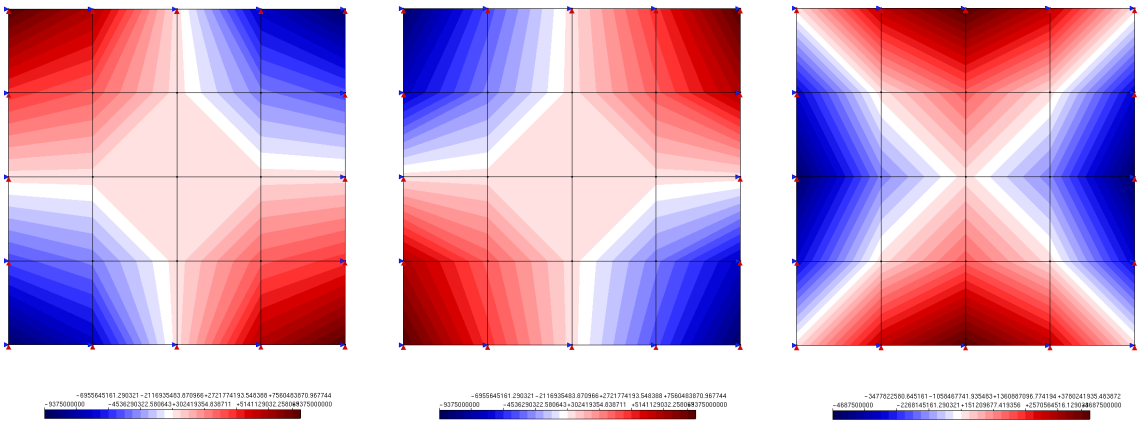

(a) σ_{11} (b) σ_{22} (c) σ_{12}

Figure 15. Stresses σ_{11}, σ_{22} e σ_{12} in the homogeneous RVE for $\gamma_{\langle 12\rangle} = 0.05$.

After all six tests, the resulting constitutive matrix, $\mathbf{C}$, that relates stresses and couple stresses to strains and microcurvatures at the macroscale, organized as in equation (21), was the following:

$$\mathbf{C} = \begin{bmatrix} 2.083 \cdot 10^{10} & 4.167 \cdot 10^{9} & 0 & 0 & 0 & 0 \\ 4.167 \cdot 10^{9} & 2.083 \cdot 10^{10} & 0 & 0 & 0 & 0 \\ 0 & 0 & 1.667 \cdot 10^{10} & 0 & 0 & 0 \\ 0 & 0 & 0 & 1.697 \cdot 10^{10} & 0 & 0 \\ 0 & 0 & 0 & 0 & 1.697 \cdot 10^{10} & 0 \\ 0 & 0 & 0 & 0 & 0 & 5.322 \cdot 10^{11} \end{bmatrix}$$

4.2 Example 2: heterogeneous material

For the second example, a square RVE, now composed of two materials, was considered. Figure 16 illustrates the RVE, with the matrix material shown in lighter color and the inclusions in darker color.

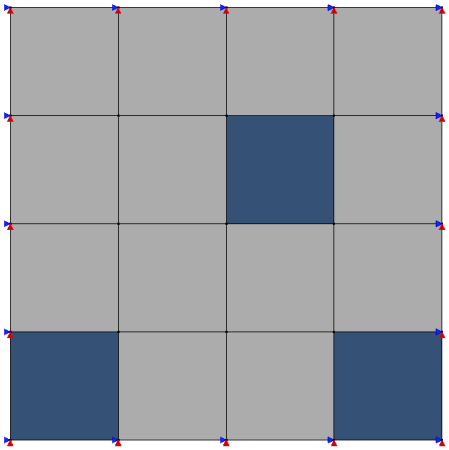

Figure 16. Heterogeneous RVE (inclusions shown in darker color).

The geometric and material properties are the following:

- length of the RVE's sides: 0.1 m;
- Young's modulus of the matrix material: $E = 5.0 \cdot 10^9$ N/m^2;
- Poisson's ratio of the matrix material: $\nu = 0.15$.
- Young's modulus of the inclusions: $E = 3.0 \cdot 10^{10}$ N/m^2;
- Poisson's ratio of the inclusions: $\nu = 0.3$.

Submitting the RVE to the condition of $\gamma_{(11)} = 1$, the contour of its deformed shape is the same observed for the first example (figure 4). However, the displacement field inside the RVE is different than that of example 1, due the different stiffness of the matrix and the inclusions. Figures 17 and 18 show, respectively, the spatial configuration of the RVE and the stresses variation inside.

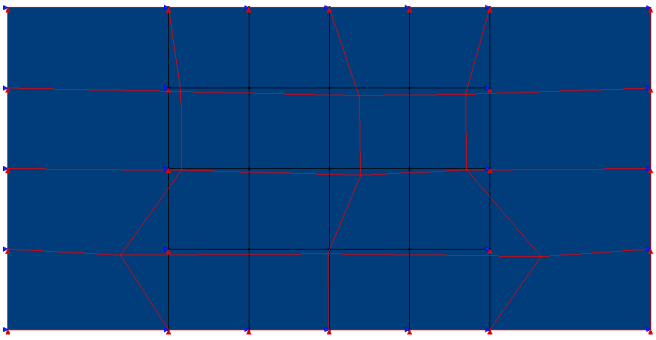

Figure 17. Spatial configuration of the heterogeneous RVE for $\gamma_{(11)} = 1$.

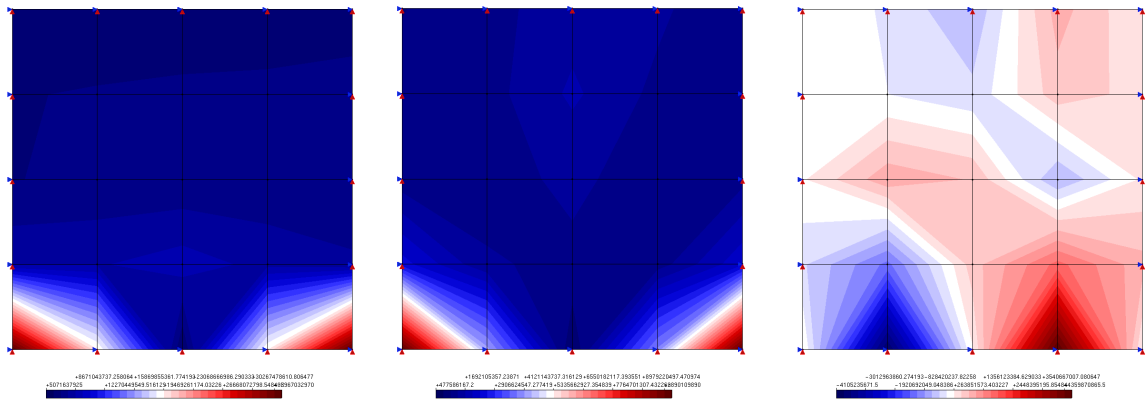

(a) σ_{11} (b) σ_{22} (c) σ_{12}

Figure 18. Stresses σ_{11}, σ_{22} e σ_{12} in the heterogeneous RVE for $\gamma_{(11)} = 1$.

For the second test ($\gamma_{(22)} = 1$), the body's deformed shaped is shown in figure 19 and the stresses are shown in figure 20.

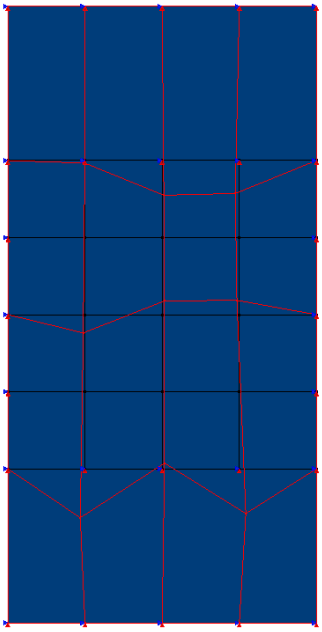

Figure 19. Spatial configuration of the heterogeneous RVE for $\gamma_{(22)} = 1$.

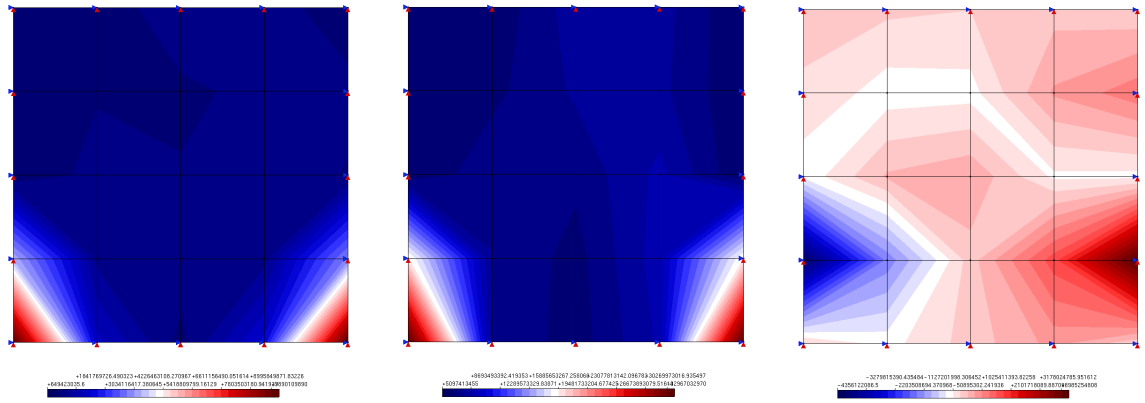

(a) σ_{11} (b) σ_{22} (c) σ_{12}

Figure 20. Stresses σ_{11}, σ_{22} e σ_{12} in the heterogeneous RVE for $\gamma_{(22)} = 1$.

When, on the third test, $\gamma_{(12)}$ was assumed equal to 0.5, the spatial configuration of the body was that of figure 21, and figure 22 shows the stresses variation throughout the RVE.

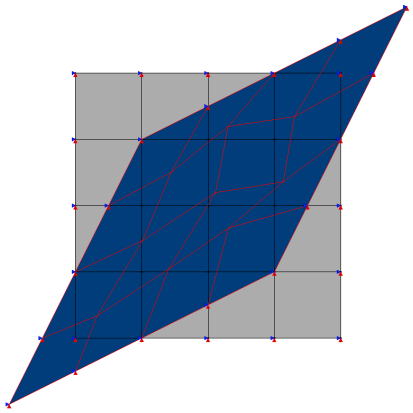

Figure 21. Spatial configuration of the heterogeneous RVE for $\gamma_{(12)} = 0.5$.

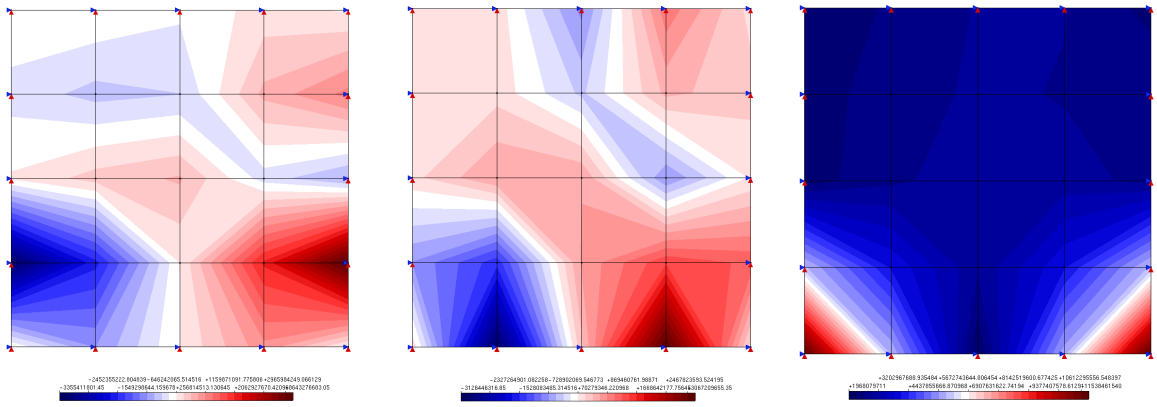

(a) σ_{11} (b) σ_{22} (c) σ_{12}

Figure 22. Stresses σ_{11}, σ_{22} e σ_{12} in the heterogeneous RVE for $\gamma_{(12)} = 0.5$.

On the fourth test, $\kappa_{13} = 1$ resulted in the deformed configuration presented in figure 23 and in the stresses presented in figure 24.

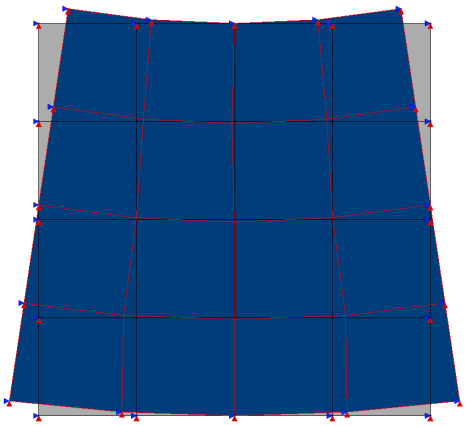

Figure 23. Spatial configuration of the heterogeneous RVE for $\kappa_{(13)} = 1$.

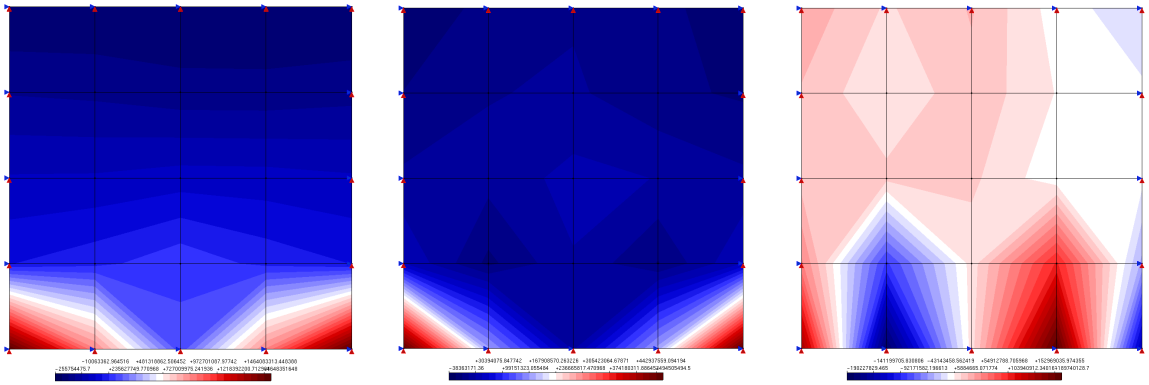

(a) σ_{11} (b) σ_{22} (c) σ_{12}

Figure 24. Stresses σ_{11}, σ_{22} e σ_{12} in the heterogeneous RVE for $\kappa_{(13)} = 1$.

Similarly, after the fifth test ($\kappa_{23} = 1$) the RVE resulted in the spatial configuration and in the stresses seen on figures 25 and 26.

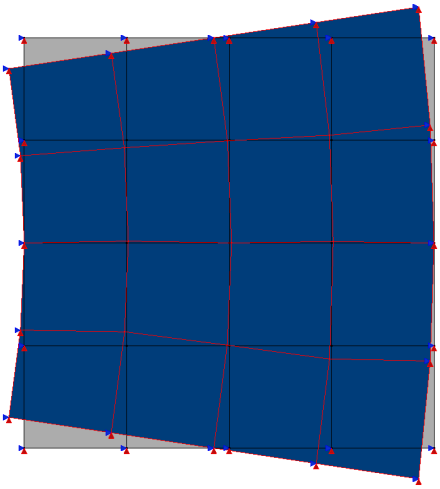

Figure 25. Spatial configuration of the heterogeneous RVE for $\kappa_{(23)} = 1$.

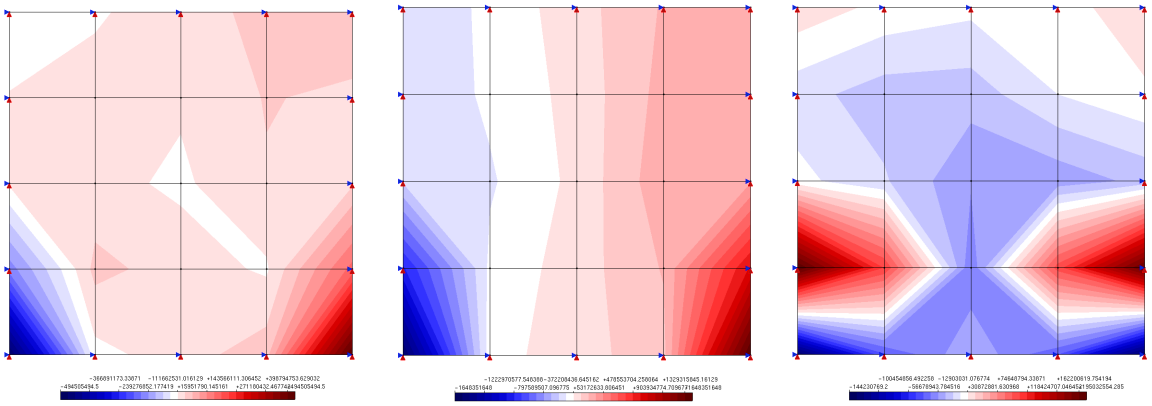

(a) σ_{11} (b) σ_{22} (c) σ_{12}

Figure 26. Stresses σ_{11}, σ_{22} e σ_{12} in the heterogeneous RVE for $\kappa_{(23)} = 1$.

On the sixth test it was used $\gamma_{\langle 0.5 \rangle} = 0.05$, and the RVE's resulting spatial configuration and stresses variation are shown in figures 27 and 28.

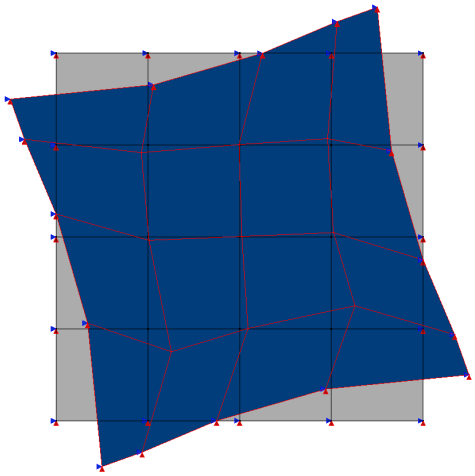

Figure 27. Spatial configuration of the heterogeneous RVE for $\gamma_{\langle 12 \rangle} = 0.05$.

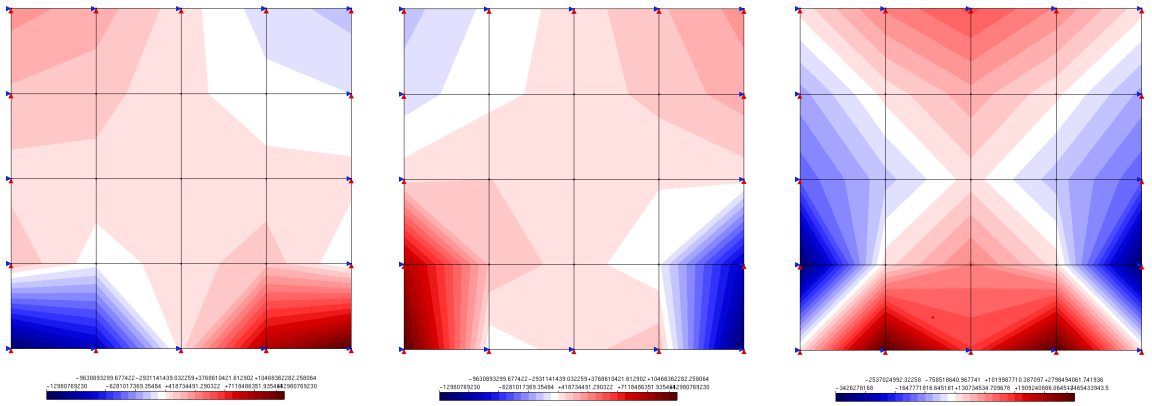

(a) σ_{11} (b) σ_{22} (c) σ_{12}

Figure 28. Stresses σ_{11}, σ_{22} e σ_{12} in the heterogeneous RVE for $\gamma_{\langle 12 \rangle} = 0.05$.

After all six tests, the resulting constitutive matrix, $\mathbf{C}$, that relates stresses and couple stresses to strains and microcurvatures at the macroscale was the following:

$$\mathbf{C} = \begin{bmatrix} 8.016 \cdot 10^9 & 1.531 \cdot 10^9 & 5.560 \cdot 10^7 & 8.700 \cdot 10^7 & -2.287 \cdot 10^5 & -4.895 \cdot 10^8 \\ 1.531 \cdot 10^9 & 8.116 \cdot 10^9 & -1.848 \cdot 10^7 & 2.222 \cdot 10^7 & 9.087 \cdot 10^6 & 2.034 \cdot 10^8 \\ 2.778 \cdot 10^7 & -9.278 \cdot 10^6 & 6.674 \cdot 10^9 & 4.076 \cdot 10^5 & 1.355 \cdot 10^7 & 1.394 \cdot 10^8 \\ 8.550 \cdot 10^7 & 2.202 \cdot 10^7 & 8.112 \cdot 10^5 & 8.167 \cdot 10^6 & 1.261 \cdot 10^4 & 9.335 \cdot 10^6 \\ -1.935 \cdot 10^5 & 9.140 \cdot 10^6 & 2.793 \cdot 10^7 & 1,348 \cdot 10^4 & 8.187 \cdot 10^6 & -6.560 \cdot 10^8 \\ -2.433 \cdot 10^8 & 1.027 \cdot 10^8 & 1.395 \cdot 10^8 & 5.141 \cdot 10^6 & -3.394 \cdot 10^8 & 2.890 \cdot 10^{11} \end{bmatrix}$$

5 Discussion of results and final comments

The theoretical study on the micropolar continuum and homogenization techniques, associated with the examples of the previous section, helped to consolidate the strategy presented in this work. In section 4.1, the analysis of an homogeneous microstructure, was interesting to validate the formulation proposed once, in this case, the behaviour is more intuitive, therefore making it easier to interpret the results obtained.

In section 4.2, the objective was to show the applicability of the proposed strategy to heterogeneous media. An important step for the evolution of this work is the automation of the process of applying the RVE's boundary conditions, which will allow the use of much finer meshes than those presented here. With finer meshes, it is possible to represent in detail diverse compositions of heterogeneous materials.

It would also be of practical interest to automate the process of computing the components of the constitutive tensors of the homogenized material. That would allow the study of the size of the RVE by analyzing different compositions in elements of different sizes, evaluating the convergence of the constitutive parameters obtained as the size of the representative element is changed.

Considering the analysis of heterogeneous media with components of various shapes described in detail, very refined meshes may be necessary. Also, triangular element meshes may be more appropriate than quadrilateral element meshes. In next studies, it will be analysed which mesh is more refined and should, therefore, be used in the homogenization process: the one that allows a detailed morphological description of the material's heterogeneity or the one that results in the convergence of the constitutive tensor.

6 Acknowledgments

The authors acknowledge the support of the Brazilian research agencies FAPEMIG (in portuguese: *Fundação de Amparo à Pesquisa do Estado de Minas Gerais*), CAPES (in portuguese: Coordenação de Aperfeiçoamento de Pessoal de Nível Superior) and CNPq (in portuguese: Conselho Nacional de Desenvolvimento Científico e Tecnológico).

References

[1] Fuina, J. S., 2009. *Formulações de Modelos Constitutivos de Microplanos para Contínuos Generalizados*. PhD thesis, Universidade Federal de Minas Gerais, Belo Horizonte, MG, Brasil.

[2] Eringen, A. C., 1999. *Microcontinuum Field Theories: I. Foundations and Solids*. Sringer New York, New York, NY, USA.

[3] Trovalusci, P., Ostoja-Starzewski, M., Bellis, M. L. D., & Muralli, A., 2014. Scale-dependent homogenization of random composites as micropolar continua. *European Journal of Mechanics A/Solids*, vol. 49, pp. 396–407.

[4] Monteiro, H. A. S., Pitangueira, R. L. S., & Barros, F. B., 2017. Multiscale strategy fot the analysis of softening media using the generalized finite element method. *XXXVIII CILAMCE - Iberian Latin-American Congress on Computational Methods in Engineering*, vol. 49, pp. 396–407.

[5] Lemaitre, J. & Desmorat, R., 2005. *Engineering damage mechanics: ductile, creep, fatigue and brittle failures*. Springer, 1 edition.

[6] Zohdi, T. I. & Wriggers, P., 2001. Computational micro-macro material testing. *Archives of Computational Methods in Engineering*, vol. 8, pp. 131–228.

[7] Hill, R., 1963. Elastic properties of reinforced solids: Some theoretical principles. *Journal of the Mechanics and Physics of Solids*, vol. 11, pp. 357–372.

[8] Chen, H., Liu, X., Hu, G., & Yuan, H., 2009. Identification of material parameters of micropolar theory for composites by homogenization method. *Computational Materials Science*, vol. 46, pp. 733–737.

[9] Forest, S. & Sab, K., 1998. Cosserat overall modeling of heterogeneous materials. *Mechanics Research Communications*, vol. 25, pp. 449–454.